Examination of Efficiency Dependence on Deceleration Voltage in a Traveling Wave Direct Energy Converter Simulator*)

Hiromasa TAKENO, Kazuhiro SHIBATA, Satoshi NAKAMOTO,
Takeru FURUKAWA and Yousuke NAKASHIMA[1)]

Kobe University, Kobe 657-8501, Japan
[1)]*University of Tsukuba, Tsukuba 305-8577, Japan*

(Received 5 January 2023 / Accepted 8 May 2023)

As for traveling wave direct energy converter (TWDEC), which was expected to be an efficient energy recovery device for fast protons created in D-^{3}He fusion, efficiency dependence on deceleration voltage was examined. A decelerator was designed based on the theory of constant deceleration scheme, in which ions were trapped in a decelerated traveling wave potential, and a simulation experiment was performed. Over a certain deceleration voltage, deceleration efficiency degraded when deceleration voltage increased, which was contradictive to the theory. Numerical orbit calculation revealed that the trapped ion exhibited the expected bouncing motion for a very short period and exited the decelerator just after acceleration phase and this caused the degradation of the deceleration effect. In the design of the decelerator, bouncing motion as well as trapping should be considered.

Keywords: advanced fusion, direct energy conversion, TWDEC, decelerator, constant deceleration

DOI: 10.1585/pfr.18.2405053

1. Introduction

Traveling wave direct energy converter (TWDEC) was proposed as an efficient device to recover fast protons created by D-^{3}He fusion [1, 2]. It consists of a modulator and a decelerator. Fast protons incident to TWDEC are velocity-modulated in the modulator and bunched in the downstream. They flow into the decelerator where a lot of electrodes are aligned in the axial direction. An external circuit is connected to the electrodes where current is induced by the protons. As a result, traveling electrostatic field is created, and the protons are decelerated by the field. The proton energy is recovered as electricity in the circuit. According to one-dimensional numerical simulation [3], about 80 % of the proton energy was recovered by TWDEC. Moreover, totally 90 % conversion efficiency can be expected if a conventional electrostatic direct current energy converter was added in the downstream of the TWDEC.

Recently, TAE technology is pursuing the p-B fusion by FRC. If produced three alpha particles have the equal energy, this method could be used for a p-B FRC reactor. But at present, as the emitted energy of alpha particles in p-B fusion is not known accurately [4], it is too early to discuss to use this method. Situation is different in the case of D-^{3}He 14 MeV protons proposed for ARTEMIS with D-^{3}He ignition [2]. However, it may be difficult to extract 14 MeV proton for direct conversion in FRC with D-^{3}He ignition because it should be used for heating plasmas. No extra margin for energy conversion is foreseen at present in D-^{3}He FRC. Therefore, D-^{3}He FRC should be operated in NBI driven mode to allow direct loss of 14 MeV proton. This concept is very close to a p-B FRC reactor originally proposed by N. Rostoker [5]. To utilize this traveling wave energy converter for fusion, an NBI driven D-^{3}He FRC reactor may be the first choice, which is desirable to be actively tackled by other fusion research group.

The authors have been carried out experimental studies of TWDEC. In the early studies, the decelerator was designed according to optimum deceleration scheme [6]. Later, constant deceleration scheme was adopted and a deceleration efficiency was extremely improved [7]. The modulation scheme was also improved, and a deceleration efficiency over 50 % was achieved [8].

The effectiveness of the constant deceleration scheme was confirmed, so we proceed to the optimization of the scheme. In this paper, we examine efficiency dependence on deceleration voltage. We examine the dependence on deceleration voltage in an experimental simulator designed based on the constant deceleration scheme. The results are discussed by employing an orbit calculation.

The contents of the paper are as follows. In Sec. 2, the constant deceleration scheme is briefly reviewed. Our experimental simulator is explained in Sec. 3. In Sec. 4, experimental results are presented, and discussion with orbit calculation is shown in Sec. 5. The conclusion is given in Sec. 6.

author's e-mail: takeno@eedept.kobe-u.ac.jp
*) This article is based on the presentation at the 31st International Toki Conference on Plasma and Fusion Research (ITC31).

2. Constant Deceleration Scheme

Before presentation of our study, we explain the theory of constant deceleration scheme briefly, the detail of which is in Ref. 3. The basic concept of this scheme is as follows. An electrostatic traveling wave is created in the decelerator, the phase velocity of which varies with constant deceleration. The ions are trapped in the potential valley of the wave, and decelerated together with the wave.

The motion of ion is illustrated in Fig. 1 (a). The axial position z is transformed to the coordinate θ moving with the traveling wave by $\theta/2\pi = (z - z_b)/\lambda$, where z_b and λ are position of the potential bottom and wavelength of the wave, respectively. The ion receives both inertia and electric force and they are balanced at the standing point $\theta = \theta_s$. Note that θ_s depends on inertia, and thus deceleration. It also depends on potential gradient, and thus height of wave potential. The ion with an appropriate velocity is trapped in the potential valley, and exhibits bouncing motion around the standing point.

The trapping condition can be discussed by a phase diagram which is shown in Fig. 1 (b). The abscissa is the position of the ion $\theta/2\pi$ and the ordinate is proportional to relative velocity of the ion $\delta u = (v - v_{ph})/v_0$, where v, v_{ph}, and v_0 are ion velocity, phase velocity of the traveling wave, and initial ion velocity before incidence into TWDEC, respectively. The ordinate is inversely proportional to squareroot of normalized amplitude of the wave potential $\Psi = eU_d/2E_0$, where e, U_d, and E_0 are unit charge, amplitude of potential in the decelerator, and initial ion energy before incidence into TWDEC, respectively. All ions in the decelerator can be described in this diagram.

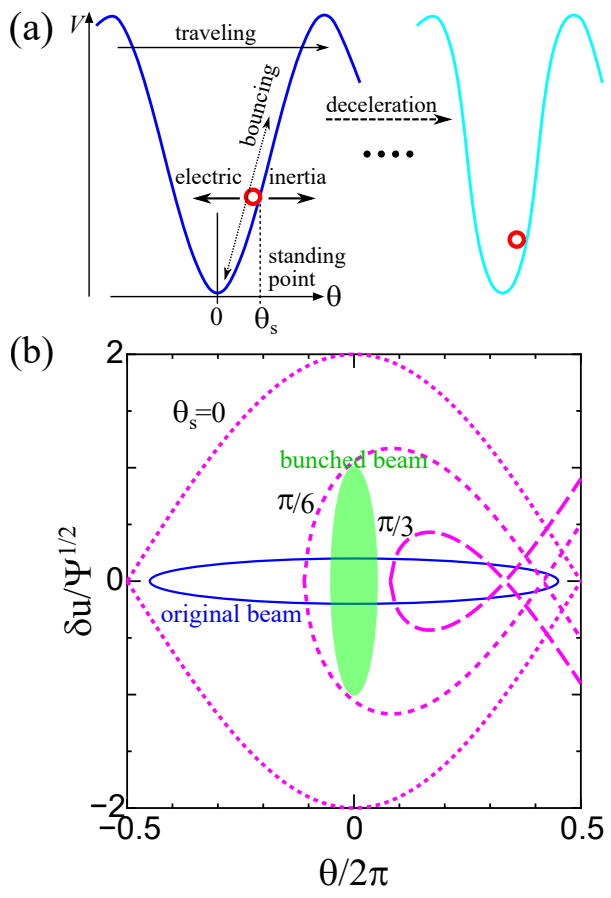

Fig. 1 Explanation of constant deceleration scheme. Illustration of ion motion (a) and trapping region in phase space (b).

In the diagram, the trapping condition is shown by closed region depending on θ_s. In Fig. 1 (b), three cases of $\theta_s = 0, \pi/6, \pi/3$ are described by different broken curves. When U_d increases, standing point θ_s balancing with the same inertia decreases, so the trapping region expands and the number of trapped ions increases. In the standard scenario to design a TWDEC, velocity modulation moves incident ions from the open oval to the filled oval in the figure, and an appropriate decelerator voltage is set to surround a large part of ions in the phase space. We can expect higher deceleration efficiency by larger U_d.

3. Experimental Equipment

The experimental simulator is schematically shown in Fig. 2. It consists of an ion source, a modulator, a decelerator, and a measurement section. The ion source is composed of a glass tube, and other sections are in a stainless steel chamber with a length about 1 m and a diameter of 35 cm. They are arranged coaxially. All RF sources are operated with amplitude modulation by 667 Hz repetitive pulse with 67 % duty ratio.

In the ion source, a helium plasma is inductively generated by an RF power of 15 MHz. An extraction voltage V_{ex} is applied to an extraction electrode at the end of the ion source, and $V_{ex} = 3.2$ kV in the present experiment. For beam convergence, a cylindrical electrode in the downstream is used by applying V_c.

In the modulator, we adopt the dual-frequency modulation method, which was proposed to improve ion bunching [9]. The actual structure contains four coaxial disk electrodes (M_1-M_4) with a hole of 6 cm diameter covered by mesh. A sinusoidal wave voltage of 7 MHz (V_{m1}) and a synchronized one of 14 MHz with leading phase difference of $\pi/2$ rad (V_{m2}) are applied to M_2 and M_3 electrodes, respectively, and other electrodes are grounded. The axial

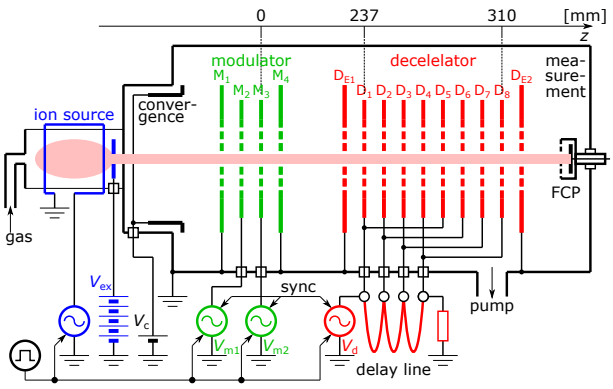

Fig. 2 Schematic illustration of experimental simulator.

intervals between electrodes are the same as the running length of the ions in a quarter period of 7 MHz. The position of M_3 is taken to be an origin of the axial coordinate.

In this study, formation of traveling wave in the decelerator is achieved by application of external RF voltages (V_d) instead of induction by bunched ions. This is a conventional manner called 'active decelerator' [6]. A 7 MHz signal synchronized with V_{m1} is amplified as V_d. The phase difference between V_{m1} and V_d is controlled appropriately to obtain the best deceleration effect.

We design the decelerator based on the constant deceleration scheme [3]. The axial position of electrodes corresponding to $\pi/2$ phase interval is determined by deceleration α, which is taken to be $\alpha = 7.8 \times 10^{11}$ m/s^2 in this study. We settled 8 electrodes $D_1 \sim D_8$ similar to those in the modulator between two grounded electrodes D_{E1} and D_{E2}. Each $\pi/2$ lagging voltage obtained by V_d and delay lines is supplied to the decelerator electrodes.

At the end of the device, a Faraday cup (FCP) is installed to analyse energy distribution of the ion beam passing through the TWDEC. The signal of the FCP is averaged by a boxcar integrator. The distribution function of the ions $f(E)$ is given by $f(E) = V_R^{-1/2}\, dI_c/dV_R|_{V_R=E/e}$, where V_R, I_c, and E mean ion repeller voltage, collector current, and ion energy, respectively. The average energy of the ions is given by $\langle E\rangle = \int_0^\infty E \cdot f(E)dE / \int_0^\infty f(E)dE$. The deceleration effect is evaluated by the deceleration efficiency defined by $R_{dec} = (\langle E_0\rangle - \langle E\rangle)/\langle E_0\rangle$, where $\langle E_0\rangle$ means the average energy of incident ions without modulation and deceleration.

4. Experimental Results

The experiment was performed under the conditions of $V_{ex} = 3.2$ kV, $V_{m1} = 200\,V_{0-p}$, and $V_{m2} = 100\,V_{0-p}$, where subscript 0-p denotes zero-to-peak and is corresponding to an amplitude of RF. By varying V_d, $f(E)$ was measured. Figures 3 (a), (b), and (c) show measured $f(E)$ for $V_d = 200\,V_{0-p}$, $300\,V_{0-p}$, and $400\,V_{0-p}$, respectively. All $f(E)$ in the figure show distribution in a wide range. There are accelerated components over 3.2 keV, and these components are ions incident in the acceleration phase. According to the figures, $f(E)$ for $V_d = 300\,V_{0-p}$ shows larger value in the lower energy region compared with that for $V_d = 200\,V_{0-p}$. This is natural as the ions trapped in the potential valley increase as V_d increases. For $V_d = 400\,V_{0-p}$, however, distribution moves in the higher energy region than the $V_d = 300\,V_{0-p}$ case although V_d increases.

The deceleration efficiency R_{dec} is evaluated, and is shown as a dependence on V_d in Fig. 4. In the figure, results of orbit calculation are also indicated, which are explained in the next section. Filled circles show experimental results. According to the figure, R_{dec} increases as V_d increases in the range of $V_d \le 300\,V_{0-p}$, however, it decreases in the range of $V_d \ge 300\,V_{0-p}$. This variation is not

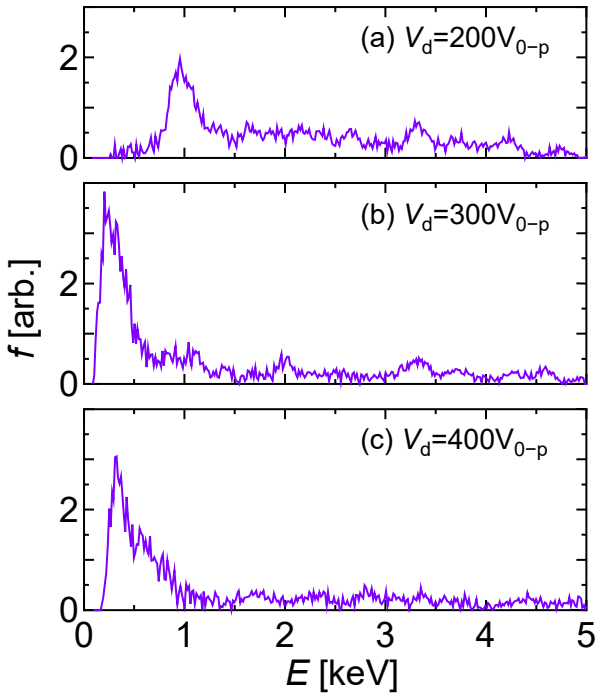

Fig. 3 Measured energy distribution functions.

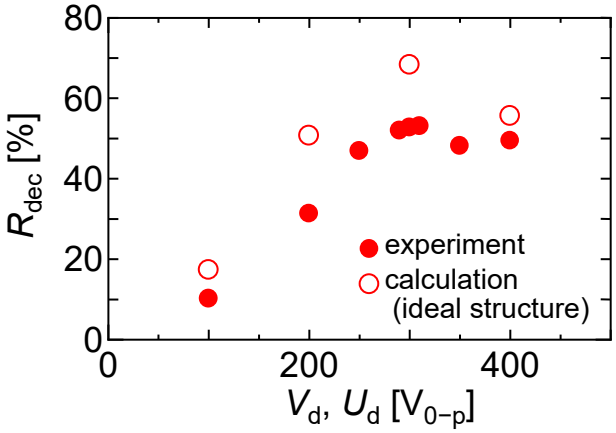

Fig. 4 Deceleration efficiency versus deceleration voltage. Filled circles and open circles are for experiment and orbit calculation, respectively.

due to accelerated high energy ions. We cannot find significant increase of the components over 3.2 keV in Fig. 3. The variation of R_{dec} must be due to the move of decelerated low energy ions and is consistent with the result in Fig. 3.

According to the theory of constant deceleration scheme, increase of V_d reduces θ_s and the trapping region expands. Then the number of trapped ions increases, which results in an increase of R_{dec}. The results shown in Figs. 3 and 4 are contradictive to the theory.

5. Discussion

We analyse the experimental result by employing one-

dimensional orbit calculation. The calculation code is the same one as before [6]. Ions with energy broadening are incident in TWDEC at a constant rate. They are affected by only given RF fields in TWDEC, and space charge effect is not taken into account. Modulation fields between electrodes are uniform in the calculation. Deceleration fields between electrodes are also uniform in the experiment. In the calculation, however, analytically expressed ideal field of constant deceleration theory is given from D_1 to D_8. This is because we will clarify the experimental result is essential to the constant deceleration scheme itself. The potential in the decelerator is given by $\psi_d(t,z) = U_d \sin\left\{\omega t + \phi_0 - \frac{\omega}{\alpha}\left[v_0 - \sqrt{v_0^2 - 2\alpha(z - z_{d1})}\right]\right\}$, where ω, t, and ϕ_0 are angular frequency, time, and initial phase, respectively, and z_{d1} is the axial position of the entrance of the decelerator which corresponds to that of the electrode D_1 in the experiment.

The conditions corresponding to V_{ex}, V_{m1}, and V_{m2} in the experiment are used, and U_d are changed according to V_d. We can evaluate $\langle E \rangle$, and hence R_{dec}, by direct calculation of average energy of all ions passing through TWDEC. Open circles in Fig. 4 shows R_{dec} versus U_d in the orbit calculation. The dependence is quite similar to that in the experiment shown by filled circles in Fig. 4 although absolute values of R_{dec} in the orbit calculation are larger than those in the experiment. The difference of the absolute values may be due to mis-alignment of the electrode structure of the decelerator, spatial potential distribution in the decelerator, and some assumptions in the calculation model, such as one-dimension, no treatment of charge potential, no treatment of particle-mesh collision and collision between particles. Although the difference should be examined in future, we concentrate the qualitative dependence in this paper. R_{dec} decreases in higher deceleration voltage, which is common to experiment and calculation, and is contradictive to the deceleration theory. By the examination of the orbit calculation, we will know the cause of the experimental result contradictive to the theory.

The condition of trapping is examined at first. The position and velocity of ions at the entrance of the decelerator can be translated into relative position θ and relative velocity δu, respectively. Those values are plotted in the phase diagram of Fig. 5. Here, (a) and (b) are for $U_d = 300\,V_{0-p}$ and $400\,V_{0-p}$, respectively. Filled red circles in (a) and open blue circles in (b) are location of ions and green curves show boundaries of trapping region. In the present condition, θ_s =1.31 rad and 0.81 rad for $U_d = 300\,V_{0-p}$ and $400\,V_{0-p}$, respectively. According to the figure, small part of ions are in the trapping region for $U_d = 300\,V_{0-p}$, however, large part of ions are in the trapping region for $U_d = 400\,V_{0-p}$. So long as we examine the trapping condition, larger deceleration effect is expected for $U_d = 400\,V_{0-p}$.

We further examine motion of each ion. We trace ion orbits for three cases of U_d. These ions locate

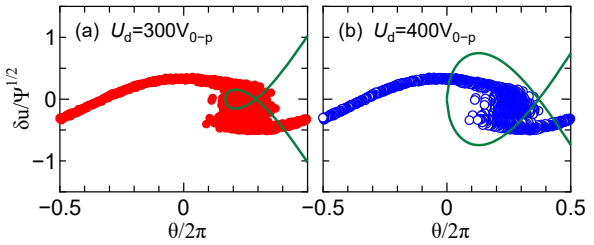

Fig. 5 Relation between ion distribution and trapping region in phase space at the entrance of the decelerator.

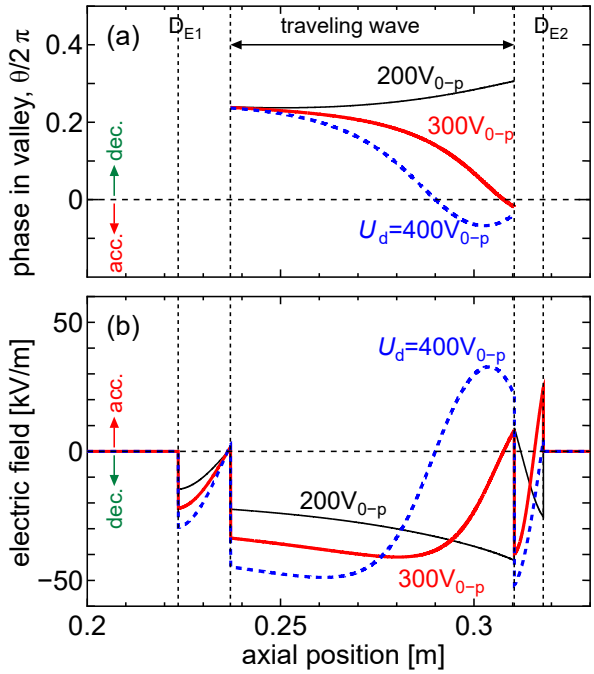

Fig. 6 Change of phase in valley and received electric field of the ion.

$(\theta/2\pi, \delta u/\Psi^{1/2}) = (0.24, -0.11 \sim -0.15)$ at the entrance of the decelerator. For $U_d = 300\,V_{0-p}$ and $400\,V_{0-p}$, they are in the trapping region.

Figures 6 (a) and (b) show change of phase in valley θ and received electric field of the ion. The abscissa of both graphs is the axial position, and the decelerator locates from 0.237 m to 0.31 m. Three cases of U_d are indicated. The bottom of the potential corresponds to $\theta = 0$, so positive and negative θ mean decelerating and accelerating positions, respectively. The positive and negative electric fields directly cause acceleration and deceleration of ions, respectively.

For $U_d = 200\,V_{0-p}$, deceleration field is not so strong, so the velocity of the ion exceeds the wave velocity, and thus θ increases in the decelerator. For $U_d = 300\,V_{0-p}$, deceleration field is appropriate and θ decreases in the decelerator. For $U_d = 400\,V_{0-p}$, however, deceleration field is strong and θ decreases rapidly. The ion reaches the bottom of the potential ($\theta = 0$) at 0.29 m, and it proceeds in

the acceleration region thereafter. Although acceleration is also found at the end of the decelerator for $U_d = 300\,V_{0-p}$, the acceleration for $U_d = 400\,V_{0-p}$ is much intense. This difference is the cause of the contradiction to the theory that the deceleration efficiency degrades for higher deceleration voltage. The ion exhibits bouncing motion for a very short period compared with theoretical expectation. In the design of the decelerator, period of bouncing motion and deceleration time should be taken into account. As an alternative way, the modulation scheme should be improved to achieve better bunching, and the amplitude of the bouncing motion should be minimized.

6. Conclusion

Efficiency dependence on deceleration voltage of TWDEC was examined. In a deceleration experiment based on the theory of constant deceleration scheme, degradation of deceleration efficiency was observed when deceleration voltage increased, which was contradictive to the theory. A numerical orbit calculation explained that the cause of degradation was termination of the bouncing motion with strong acceleration. Not only trapping, but also bouncing motion should be considered in the design of decelerator.

Acknowledgment

The authors acknowledge valuable discussions with Drs. J. Miyazawa and T. Goto. This work is supported in part by a Grant-in-Aid for Scientific Research (20H02131) from JSPS and is also supported in part by the bilateral coordinated research between PRC, Univ. Tsukuba, NIFS, and Kobe Univ (NIFS13KUGM082).

[1] H. Momota, LA-11808-C, Los Alamos Natl. Lab., 8 (1990).
[2] H. Momota *et al.*, Proc. 7th Int. Conf. on Emerging Nucl. Energy Systems, 16 (1993).
[3] H. Katayama and K. Sato, J. Plasma Fusion Res. **77**, 698 (2001) (in Japanese).
[4] M.C. Spraker *et al.*, J. Fusion Energy **31**, 357 (2012).
[5] N. Rostoker *et al.*, J. Fusion Energy **22**, 83 (2003).
[6] H. Takeno *et al.*, Jap. J. Appl. Phys. **39**, 5287 (2000).
[7] Y. Togo *et al.*, Plasma Fusion Res. **10**, 3405013 (2015).
[8] K. Shibata *et al.*, Plasma Fusion Res. **14**, 3405078 (2019).
[9] H. Takeno *et al.*, Plasma Fusion Res. **14**, 2405014 (2019).